Hindawi
International Journal of Polymer Science
Volume 2023, Article ID 9598572, 9 pages
https://doi.org/10.1155/2023/9598572

Research Article

Nanoporous Double-Gyroid Structure from ABC Triblock Terpolymer Thick Films

Karim Aissou,[1,2] **Maximilien Coronas**,[1] **Daniel Hermida-Merino**,[3,4] **Eduardo Solano**,[5] **Didier Cot**,[1] **Stéphanie Roualdes**,[1] **Denis Bouyer**,[1] **and Damien Quemener**[1]

[1]*Institut Européen des Membranes, IEM, UMR 5635, University of Montpellier, ENSCM, CNRS, Montpellier, France*
[2]*Laboratoire de Chimie des Polymères Organiques, University Bordeaux, CNRS, Bordeaux INP, LCPO, UMR 5629, F-33600 Pessac, France*
[3]*DUBBLE CRG BM26@ESRF, Netherlands Organization for Scientific Research (NWO), 71 Avenue des Martyrs, 38000 Grenoble, France*
[4]*Departamento de Física Aplicada, CINBIO, Universidade de Vigo, Campus Lagoas-Marcosende, E36310, Vigo, Galicia, Spain*
[5]*NCD-SWEET Beamline, ALBA Synchrotron Light Source, Cerdanyola del Vallès 08290, Spain*

Correspondence should be addressed to Karim Aissou; karim.aissou@umontpellier.fr

Received 28 March 2023; Revised 12 September 2023; Accepted 23 September 2023; Published 10 October 2023

Academic Editor: Cornelia Vasile

The creation of nanostructured materials with a triply periodic minimal surface (TPMS), defined as a zero mean curvature surface having periodicity in three-dimensional space, is an emerging solution to optimize transport (i.e., the ion-conductivity and hydraulic permeability) through the next-generation of electrolyte and ultrafiltration (UF) membranes. Here, we used an amphiphilic ABC-type block copolymer (BCP) (namely, polystyrene-*block*-poly(2-vinylpyridine)-*block*-poly(ethylene oxide) (PS-*b*-P2VP-*b*-PEO)) to generate symmetric thick films (~8 μm) composed entirely of a TPMS-based structure, consisting of a PS matrix with a double gyroid (DG) minimal surface and hydrophilic stimuli-responsive (P2VP/PEO) nanochannels. To produce the core/shell DG-structured monoliths, we used a process combining the nonsolvent-induced phase separation (NIPS) process with a solvent vapor annealing (SVA) treatment. From such symmetric ABC-type BCP-thick films generated by NIPS-SVA, a mean hydraulic permeability as high as 514 $L\,h^{-1}\,m^{-2}\,bar^{-1}$ was measured. This mean value was revealed to be nearly equal to that of asymmetric PS-*b*-P2VP-*b*-PEO membranes manufactured by NIPS, which have a substructure with an implicit irregular and random distribution of the internal pore structure and a skin layer with P2VP/PEO nanopores arranged into a hexagonal array.

1. Introduction

Improving transport in mechanically robust nanoporous membranes by creating effective pathways is very important for increasing the heat dissipation [1] as well as the ionic conduction in fuel cells [2] and batteries [3–5] or optimizing the figure of merit of separation-based materials for valuable ultrafiltration (UF) applications [6–9]. However, controlling the orientation of porous nanochannels at the scale of membrane thickness (i.e., several micrometers) remains a major challenge to avoid the formation of undesirable dead ends that limit the transport properties.

An attractive way to optimize transport within the membrane without compromising its overall mechanical properties is to use porous materials with a triply periodic minimal surface (TPMS) [10]. By definition, TPMS is a minimal surface with zero mean curvature that extends periodically in all three directions. These properties provide an excellent solution for the fabrication of advanced nanoporous membranes with controllable critical parameters (e.g., the connectivity of pathways and tortuosity) since TPMS-based structures can be precisely expressed by mathematical functions [11]. Among the different TPMS geometries, the double-gyroid (DG) is an intriguing bicontinuous phase that has recently

gained interest in improving both ion transport in energy conversion and storage devices [12–14] and water transport through UF membranes [15]. The DG structure is formed by two mutually interwoven network channels, arranged in a cubic lattice with $Ia\ \bar{3}\ d$ symmetry, where each channel is inherently interconnected in three dimensions via three-way junctions, and the very smooth gyroid minimal surface separating the two networks ensures an excellent mechanical robustness of the material.

One of the most promising approaches to produce nanoporous materials with a DG structure is to use block copolymers (BCPs) as templates since BCPs are able to self-assemble into unique cocontinuous nanostructures such as the cubic DG (space group 230) and double diamond (space group 224) phases and the orthorhombic *Fddd* (space group 70) morphology [16, 17]. Following this strategy, water transport in several nanoporous materials derived from the self-assembly of BCPs into a DG structure has been examined in the literature [15, 18, 19]. However, a selective removal of the minor block has been systematically used to create the bicontinuous porosity within UF membranes, thereby leading to hydrophobic materials that can have a limited permeability and can be more easily subject to fouling if a postmodification treatment is not applied [18].

To overcome this issue, we herein propose to use an amphiphilic ABC-type BCP (namely, polystyrene-*block*-poly(2-vinyl pyridine)-*block*-poly(ethylene oxide) (PS-*b*-P2VP-*b*-PEO)) to generate permeable core/shell DG-structured monoliths with hydrophilic stimuli-responsive (P2VP/PEO) nanochannels. To achieve a reproducible DG structure, the PS-*b*-P2VP-*b*-PEO (S:V:EO≈65 : 21 : 13, 69.5 kg.mol^{-1}) films were blended with 30 wt. % of PS-*b*-PEO (S:EO≈70 : 30, 39 kg.mol^{-1}) chains, while the DG-structured monoliths were generated by combining the nonsolvent-induced phase separation (NIPS) process with a solvent vapor annealing (SVA) treatment. Following this method, the NIPS-based terpolymer thick films, consisting of an asymmetric and highly porous sponge-like substructure topped by a dense thin layer with nanopores arranged in a hexagonal array, were exposed to a chloroform vapor to produce a well-developed DG structure within the entire film thickness. The mean hydraulic permeability value (514 L h^{-1} m^{-2} bar^{-1}) of symmetric DG-structured materials, which was favorably interpreted using the Hagen-Poiseuille law, was also compared with the mean value (690 L h^{-1} m^{-2} bar^{-1}) of their asymmetric homologues (i.e., of the same material) generated by the conventional NIPS method to evaluate the transport efficiency within the TPMS-based structure.

2. Results

The cross-sectional SEM views presented in Figure 1(a) show a 14.5 μm thick PS-*b*-P2VP-*b*-PEO/PS-*b*-PEO film blended with 30 wt. % of PS-*b*-PEO chains, which adopt an asymmetric architecture after the NIPS treatment. To generate this asymmetric and highly porous architecture, a square-shaped PS-*b*-P2VP-*b*-PEO/PS-*b*-PEO film was first drawn onto a (3 × 3 cm) silicon substrate by using a tape casting technique with a 250 μm gap from 18% wt. terpolymer solution in a disolvent mixture of 1,4-dioxane/tetrahydrofuran (DOX/THF: 80/20 by weight). The disolvent mixture was subsequently evaporated for 60 s at room temperature (RT) to form a dense air surface layer (see Figure 1(b)). The blended PS-*b*-P2VP-*b*-PEO membrane was then immersed into a heptane bath at RT for 5 min to create a sponge-like substructure (see inset). Note that a dense bottom layer is also formed at the opposite interface of the PS-*b*-P2VP-*b*-PEO/PS-*b*-PEO thick film (see Figure 1(c)). Fortunately, this undesirable dense bottom layer did not affect the water permeability capabilities of the terpolymer membrane (i.e., permeability remains high; see the water flux results discussed hereafter).

To know more about the morphology generated on the membrane top surface during the NIPS process (that is not at the equilibrium), the atomic force microscopy (AFM) technique was used. The representative (4 × 4 μm) AFM topographic view indicates that the top surface of PS-*b*-P2VP-*b*-PEO/PS-*b*-PEO thick films generated by NIPS is quite rough (see Figure S1a), while the magnified AFM topographic image presented in Figure 2(a) shows the porous P2VP/PEO (black) nanodomains are arranged into a 2D hexagonal structure with a period of ~40.1 nm. The corresponding Delaunay triangulation shows that this trivial 2D array has a high density of defects ($\rho = 0.3$) such as dislocations and disclinations that delimit small grains (see Figure 2(b)). In addition, a mean pore diameter of ~16.4 nm with a large standard deviation ($\sigma = 4.6$ nm) was also measured (see Figure S1b). These results confirm that stabilizing a long-range ordered nanostructure by using a NIPS process remains a major challenge [20].

To transform this kinetically trapped phase into a well-ordered nanostructure at equilibrium, the asymmetric NIPS-made PS-*b*-P2VP-*b*-PEO/PS-*b*-PEO thick films were exposed to a chloroform vapor for 5 h. The AFM topographic view presented in Figures 3(a) shows that a double-gyroid (DG) structure, exhibiting a typical double-wave pattern formed within large grains, is produced on the film top surface after the SVA treatment (5 h, $CHCl_3$). Interestingly, the high magnification AFM topographic image focused on a single grain orientation reveals this 3D nanostructure is well-developed since the characteristic spots of the double wave pattern, consisting of small- and large-amplitude oscillations and corresponding to the (211) crystallographic plane of the DG structure, are clearly visible on its associated bidimensional fast Fourier transform (2D-FFT) (see Figures 3(b) and 3(c)).

Moreover, the low magnification (7 × 7 μm) AFM topographic image presented in Figure S2 suggests that a preferential orientation parallel to the air surface of the (211) crystallographic plane occurs which is fully supported by the grazing incidence small-angle X-ray scattering (GISAXS) data (see Figure S3). Indeed, the GISAXS pattern corresponding to a solvent-annealed (5 h, $CHCl_3$) PS-*b*-P2VP-*b*-PEO/PS-*b*-PEO thick film well matches with the (121) and (220) Bragg diffraction spots as reported by the Lee et al. [21, 22], confirming that a preferential {121} orientation occurs within the entire film thickness of the

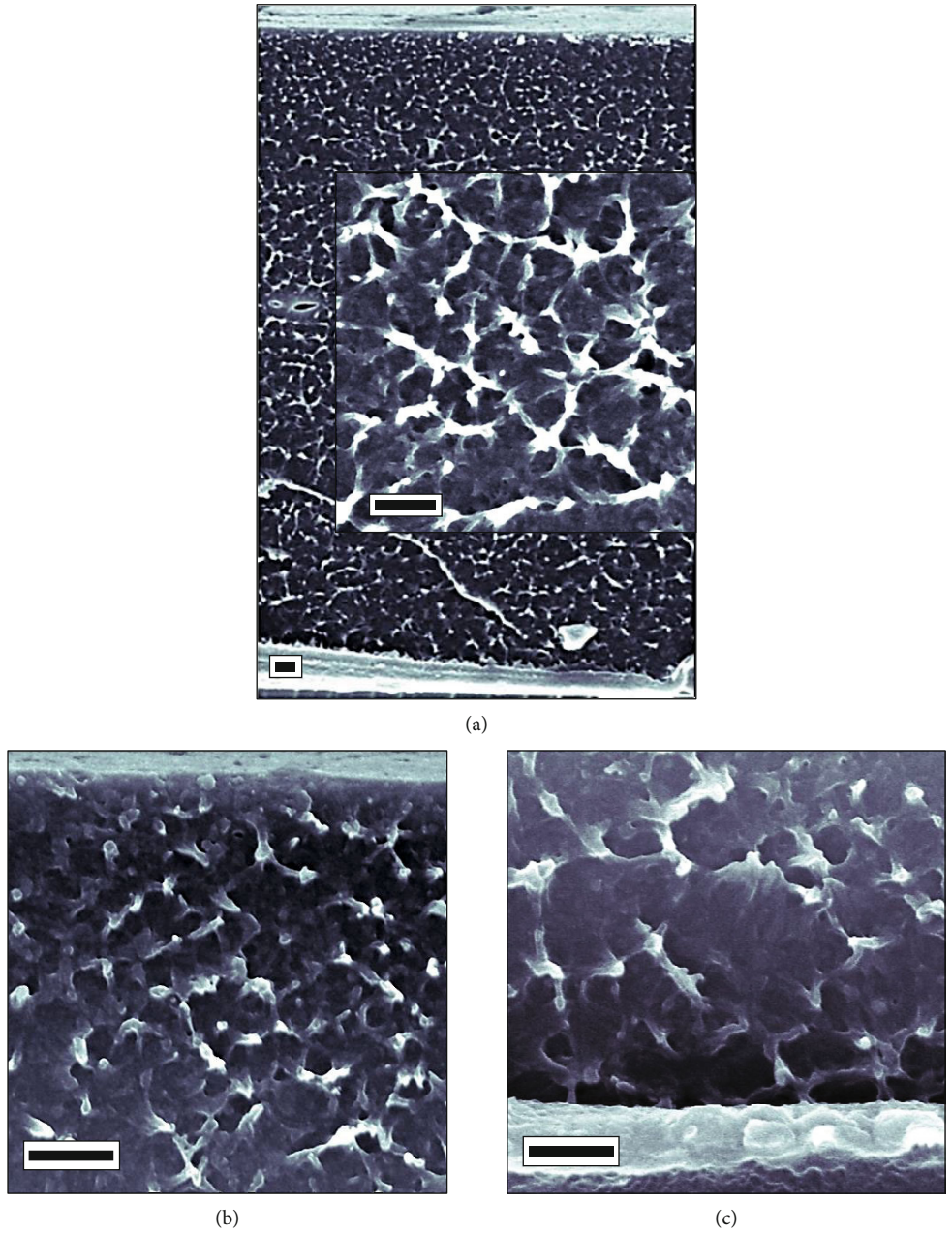

(a)

(b)

(c)

Figure 1: Cross-sectional SEM views of a PS-*b*-P2VP-*b*-PEO/PS-*b*-PEO thick film generated by NIPS showing (a) the entire material with a thickness of ~14.5 μm and the presence of a graded sponge-like substructure with small and large pores near the (b) top and (c) bottom layers, respectively. Inset: magnified SEM image of the microporous (sponge-like) substructure formed within the asymmetric terpolymer-thick film. Scale bars: 500 nm.

terpolymer material. From this GISAXS pattern, the unit cell of the DG structure (a_G) was determined to be 75.8 nm, based on the diffracted $(20\bar{2})$ peak at $q_{y,(20\bar{2})}$ ~0.234 nm^{-1} ($a_G = (2\pi \times 2\sqrt{2})/q_{y,(20\bar{2})}$), while the period of the (121) plane was estimated to be 30.9 nm.

To gain insight into the DG structure formed inside the PS-*b*-P2VP-*b*-PEO/PS-*b*-PEO thick film generated by NIPS-SVA, cross-sectional SEM images showing different regions of the terpolymer material were acquired. The cross-sectional images shown in Figure 4 indicate that the solvent-annealed (5 h, $CHCl_3$) PS-*b*-P2VP-*b*-PEO/PS-*b*-PEO thick film has lost its asymmetric architecture as well as its high porosity generated by NIPS (see Figure 1). Indeed, the blended terpolymer material strongly densified during the SVA treatment to form a symmetric film entirely composed of the DG structure as shown on the cross-sectional SEM views taken close to the top and bottom surfaces and in the middle of the blended PS-*b*-P2VP-*b*-PEO monolith (see Figures 4(a)–4(c)). It is worth noting that the densification process occurring during the SVA treatment greatly reduces the thickness of blended terpolymer monoliths since a thickness of ~8 μm was measured from SEM images. This

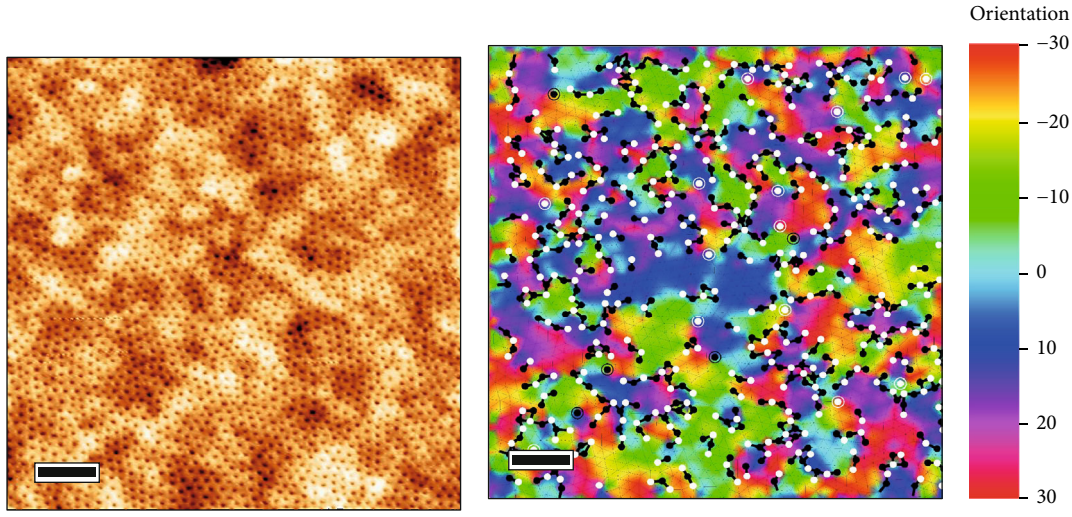

Figure 2: (a) AFM topographic image and (b) its associated Delaunay showing the top surface of a NIPS-made PS-*b*-P2VP-*b*-PEO/PS-*b*-PEO thick film. The dark (P2VP/PEO) pores are arranged into a short-range ordered hexagonal array with a period of ~40.1 nm. In the Delaunay triangulation, the small dots are six-fold coordinated pores, while the black and white big dots, indicating defect sites, are five- and sevenfold coordinated (P2VP/PEO) domains, respectively. The colormap shows the orientations of small grains (-30°–30°). Scale bars: 250 nm.

behavior has been also observed in previous studies [17, 23, 24]. Interestingly, the SEM image in Figure 4(d) shows that the DG structure on the bottom surface is not clearly visible compared to the well-developed double wave pattern produced on the top surface (see inset).

To elucidate the formation of the DG structure during the SVA treatment, an early stage of annealing under a chloroform vapor was captured. The AFM topographic view presented in Figure S4a shows that the solvent-annealed (45 min, $CHCl_3$) PS-*b*-P2VP-*b*-PEO/PS-*b*-PEO thick film produced on the top surface has a long-range ordered nanostructure exhibiting a 31 nm period wavy line pattern. This pattern differs both from the hexagonal phase generated by NIPS and the double-wave pattern observed after a longer SVA duration. In addition, it can be seen from the top-view SEM images that the blended triblock terpolymer thick film generated by NIPS-SVA (45 min, $CHCl_3$) consists of a sponge-like substructure topped by a sub-100 nm thick layer with a "wavy line and dot" pattern (see Figure S4b-c). The GISAXS data indicate this morphology generated by NIPS-SVA (45 min, $CHCl_3$) presents similarities with the DG structure, as the intensity cut along the horizontal q_y direction, taken around the Yoneda band, displays peaks that overlap the gyroid diffraction peaks at $q_y = 0.113$, 0.154, 0.177, 0.202, and $0.234\,nm^{-1}$ (see Figure S5). However, the wavy line and dot morphology, presenting epitaxial relations with the (211) DG plane (notably the same period), shows lower peak intensities than that arising from the well-developed 3D structure manufactured by NIPS-SVA (5 h, $CHCl_3$). This phenomenon is probably due to the fact that the solvent-annealed (45 min, $CHCl_3$) PS-*b*-P2VP-*b*-PEO/PS-*b*-PEO film has an asymmetric architecture with a thick sponge-like substructure (>10 μm), which undoubtedly increases the background noise during the GISAXS measurement. The presence of a sponge-like substructure occupying most of the terpolymer film thickness could also affect the formation of the double pattern since it has been demonstrated that the small and large amplitude oscillations of the (211) DG plane are well-developed only when the layer thickness is well above the size of a_G [25]. In other words, a metastable wavy line and dot phase similar to the one produced in this work was already stabilized when the film thickness was lower (or in the same range) than the unit cell dimension. Importantly, this metastable phase was also observed theoretically during the cylinder-to-DG transition using the self-consistent field theory (SCFT), which implies that the order-order transition between the hexagonal cylinder and DG structures proceeds epitaxially by a nucleation and growth mechanism [26].

As the flow rate of water through symmetric membranes composed entirely of a well-defined DG structure has rarely been reported due to the complexity of manufacturing a such porous phase, the results obtained in this study are compared with those predicted using the conventional the Hagen-Poiseuille (H-P) fluid flow theory defined as follows:

$$J = N\frac{\pi d^4 \Delta P}{128 \times \mu \times \tau \times L}, \quad (1)$$

where J is the flux, N is the areal density of pores, d is the pore diameter, ΔP is the transmembrane pressure, μ is the viscosity of water (1×10^{-3} Pa.s at 20°C), τ is the pore tortuosity ($\tau = 1.371 - 0.250 \times (1 - \phi_{PS}) + 0.086 \times (1 - \phi_{PS})^2 = 1.295$ for the gyroid structure) [11], and L is the nanochannel length (approximated here by the film thickness ≈8 μm).

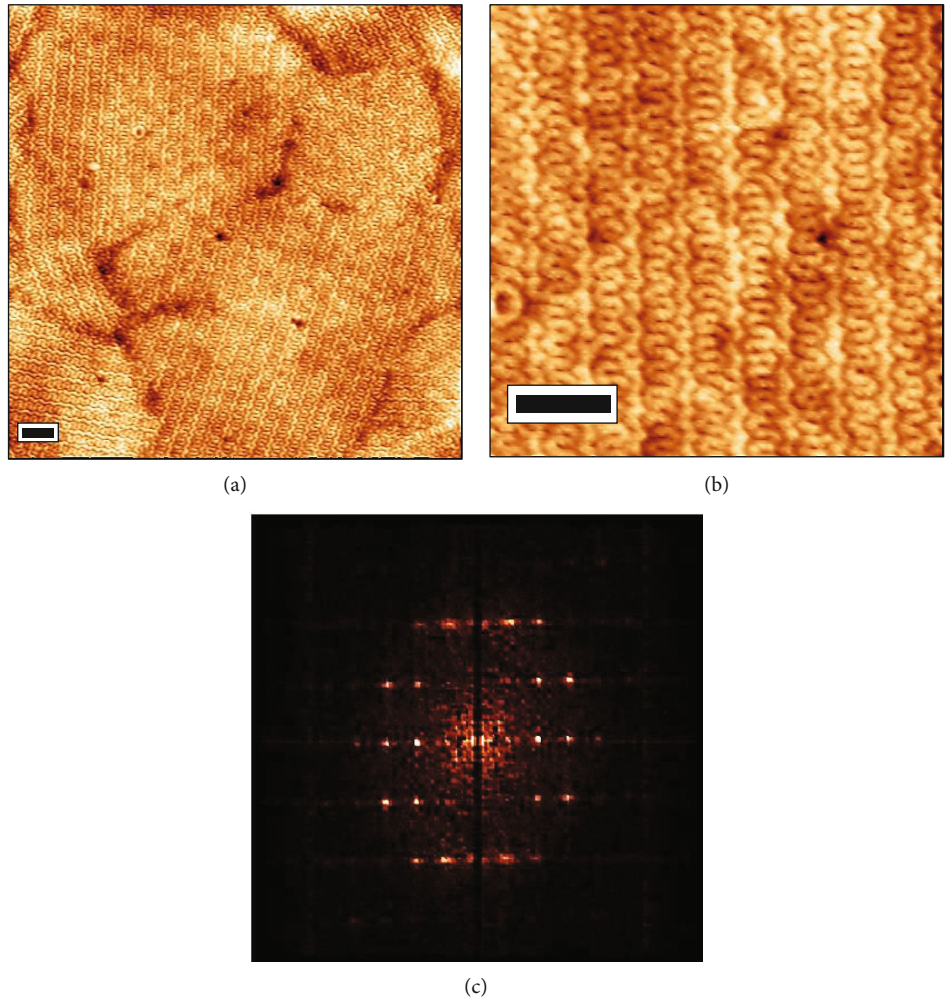

(a) (b) (c)

Figure 3: (a) Topographic AFM image of a NIPS-SVA-made (5 h, $CHCl_3$) PS-*b*-P2VP-*b*-PEO/PS-*b*-PEO thick film showing large grains formed by the DG structure on the material top surface. (b) Magnified AFM topographic view and (c) its 2D-FFT revealing the double wave pattern is well developed within its grain as the 2D-FFT exhibits sharp spots. Scale bars: 250 nm.

If we assume that the blended terpolymer monolith has a PS volume fraction, ϕ_{PS}, of ~0.66, a pore radius, R_{pore}, of ~17.7 nm ($2\pi R_{pore}^2/a_G^2 = (1-\phi_{PS})$), and thus an areal density, N, of 3.46×10^{14} pores/m^2 ($N\pi R_{pore}^2 = (1-\phi_{PS})$), it can be determined by approximating the DG morphology to two tortuous and unconnected porous nanochannels per unit cell (see Figure 5(a)). Using these parameter values, a theoretical permeability, $J/\Delta P$, of 463 L m^{-2} h^{-1} bar^{-1} can be calculated, which agrees quite well with the mean water permeance value (514 L h^{-1} m^{-2} bar^{-1}) measured from three different solvent-annealed (5 h, $CHCl_3$) terpolymer films deposited on porous (0.1 μm) hydrophilic PVDF supports (see Figure 5(b)). Note that the mean water permeance value corresponds to the slope of the linear fits based on Darcy's law, and the value of the coefficient of determination, R^2, close to unity ($R^2 \approx 0.99$) indicates that the DG-structured monoliths exhibit excellent stability to material failure even at 2 bar (water conditions: pH = 7 and $T = 20^{\circ}$C). Conversely, the mean water permeance value (690 L h^{-1} m^{-2} bar^{-1}, $R^2 \approx 0.99$) of the asymmetric terpolymer films produced by NIPS deviates strongly from the theoretical value calculated using the H-P law, indicating that the sponge-like substructure contributes strongly to the permeability (in this study of ~84%) [27]. Indeed, an asymmetric membrane architecture comprising an ideal sponge-like substructure with no resistance to water transport and a 100 nm thick top surface with porous domains packed in a 40 nm period hexagonal lattice ($N = 6.56 \times 10^{14}$ pores/m^2) would reach a theoretical value of ~4192 L m^{-2} h^{-1} bar^{-1}. In contrast to asymmetric terpolymer membranes generated by NIPS, the results show that the permeability value of the DG-structured monoliths is predictable. Moreover, this average value is also almost the same as the value measured from NIPS-based membranes since the error bars overlap.

To extend the comparison, we recently studied the permeability of blended PS-*b*-P2VP-*b*-PEO symmetric membranes composed entirely of a hexagonal perforated lamellar (HPL) phase [24]. These 9 μm-thick PS-*b*-P2VP-*b*-PEO monoliths blended with 20 wt. % of short PS chains showed a water permeance of ~30 L h^{-1} m^{-2} bar^{-1}, which is an order of magnitude lower than the mean value obtained

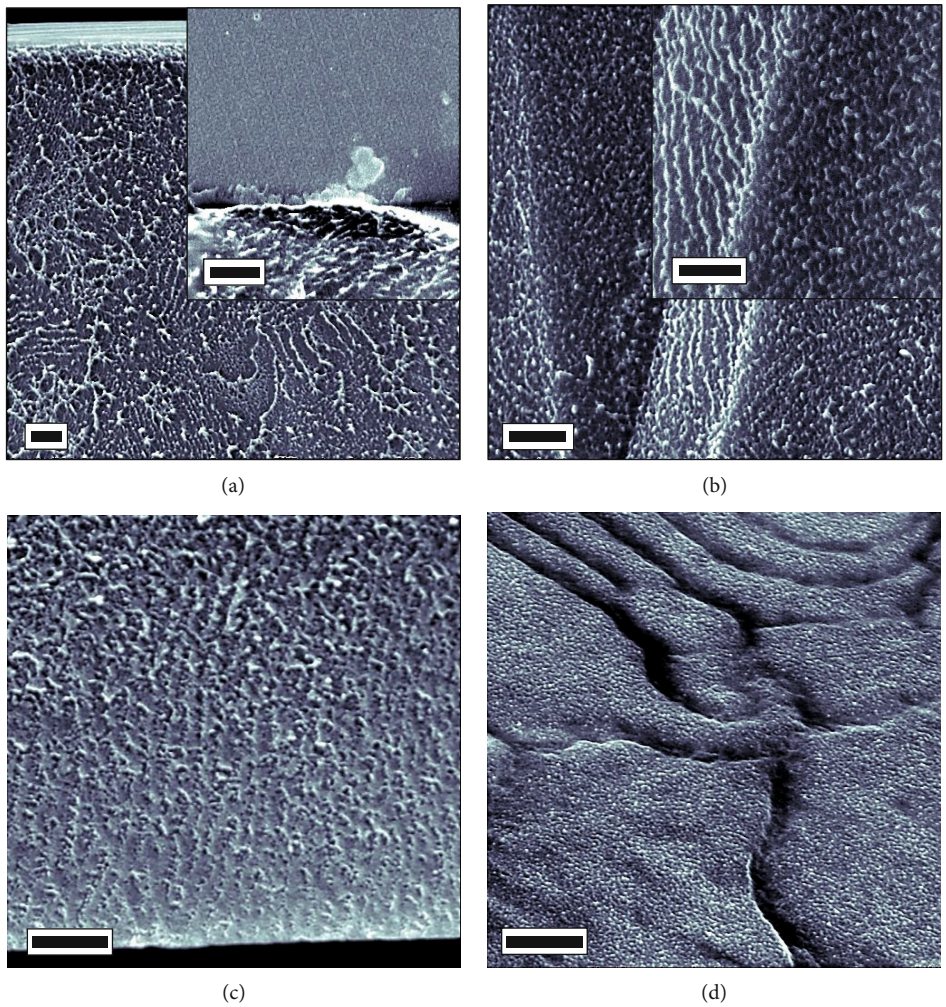

Figure 4: Cross-sectional SEM views of a PS-*b*-P2VP-*b*-PEO/PS-*b*-PEO monolith generated by NIPS-SVA (5 h, $CHCl_3$) showing the DG structure in the vicinity of the (a) top, (b) middle, and (c) bottom film regions. (d) A top-view SEM image revealing the nanoporous morphology formed on the bottom surface. Inset: top view SEM image showing the double wave pattern produced on the membrane top surface and the DG structure formed within the blended terpolymer film. Scale bars: 500 nm.

for the DG-structured monoliths studied in this work. This result confirms that the HPL phase having PS perforations is not an optimized 3D morphology to generate monoliths with efficiently interconnected porous nanochannels that are able to limit the tortuosity of the porous structure and obviate the need for domain alignment as the morphological excellence of the DG structure.

3. Conclusion

In summary, symmetric terpolymer monoliths composed entirely of a well-developed DG nanostructure were fabricated using the NIPS-SVA method. A mean average hydraulic permeance of $514\,L\,h^{-1}\,m^{-2}\,bar^{-1}$ was measured for these DG-structured monoliths, showing a linear variation between J and the pressure difference. By approximating the DG morphology to two tortuous and unconnected porous nanochannels per unit cell, we found that the mean hydraulic permeability value of such symmetric terpolymer monoliths agrees well with the theoretical value calculated using the Hagen-Poiseuille law. This permeability value was found to be an order of magnitude higher than that measured from analogous PS-*b*-P2VP-*b*-PEO membranes composed entirely of a perforated hexagonal lamellar phase (HPL). Lastly, the use of PEO-based BCP chains to create bicontinuous porosity in UF membranes is highly desirable to produce nanopores with improved fouling resistance properties.

4. Experimental

4.1. Material. 1,4-Dioxane (DOX, 99.5%), tetrahydrofuran (THF, 99%), chloroform ($CHCl_3$, 99%), poly(3,4-ethylenedioxythiophene):polystyrene sulfonate (PEDOT:PSS, 2.8% wt. in water), and PVDF membranes (Durapore, 0.1 μm and 47 mm) were purchased from Sigma-Aldrich. Silicon substrates were provided by Silicon Materials (Si-Mat). The PS-*b*-P2VP-*b*-PEO (S:V:EO $\approx$ 65 : 21 : 13, 69.5 $kg.mol^{-1}$) and PS-*b*-PEO (S:EO $\approx$ 70 : 30, 39 $kg.mol^{-1}$) BCP chains, used in this work, were purchased from Polymer Source Inc (Canada).

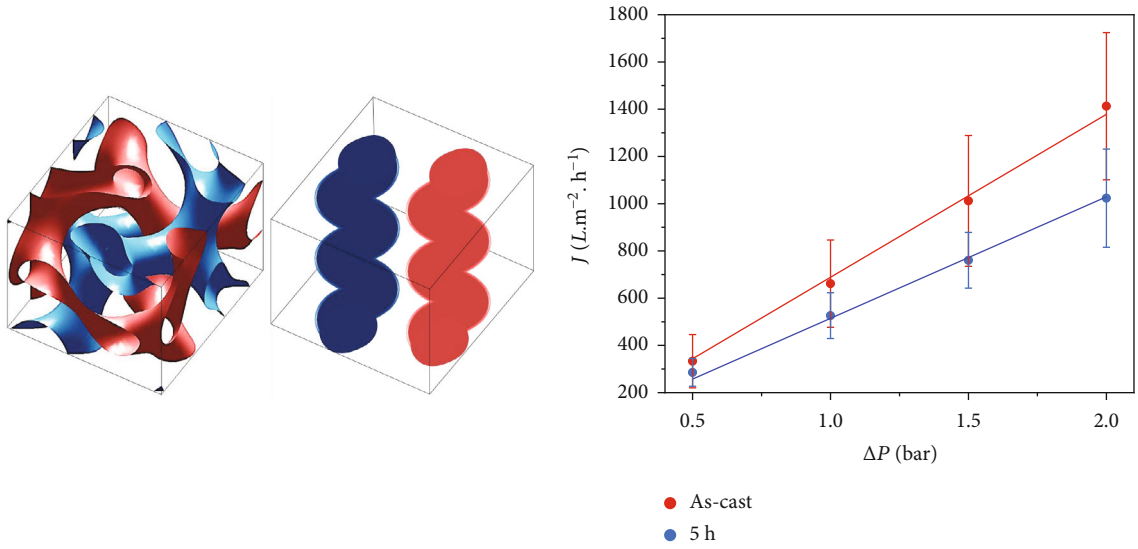

(a) (b)

Figure 5: (a) Schematic representation of the DG unit cell (a cube with sides equal to a_G) showing only the (red and blue) intermaterial dividing surfaces (IMDSs) separating the two interpenetrating three-dimensional continuous networks from the matrix (left). To apply the H-P law, each network made of interconnected tubes was simplified to a tortuous nanochannel having a circular cross-section (right). (b) Water fluxes, J, of the NIPS-made PS-*b*-P2VP-*b*-PEO/PS-*b*-PEO materials exposed to a $CHCl_3$ vapor for different times: (red dots) 0 min and (blue dots) 5 h. The error bars are the standard deviations of the mean relative flux values calculated for 3 different samples.

4.2. Asymmetric PS-b-P2VP-b-PEO/PS-b-PEO Thick Films Generated by NIPS. Asymmetric PS-*b*-P2VP-*b*-PEO films were manufactured by NIPS as follows: 18% wt. terpolymer solution in a disolvent mixture (DOX/THF: 80/20 by weight) was first prepared and heated for 30 minutes at 70°C in order to achieve the dissolution of the terpolymer. The terpolymer solution was cooled down at RT before any uses. To produce the PS-*b*-P2VP-*b*-PEO/PS-*b*-PEO films, 120 μL of the terpolymer solution was dropped onto (3×3 cm) silicon substrates and sprayed homogeneously by using a tape casting technique with a 250 μm blade. To fabricate asymmetric PS-*b*-P2VP-*b*-PEO/PS-*b*-PEO films topped by a 2D hexagonal nanoporous structure, the previously casted solution was kept in the room during the 60 s at RT to allow the solvents to evaporate, and then the terpolymer materials were immersed into a (nonsolvent) heptane bath at RT for 5 min to produce a sponge-like substructure.

4.3. DG-Structured PS-b-P2VP-b-PEO/PS-b-PEO Monoliths Generated by SVA. To achieve monoliths entirely composed of a DG structure, the terpolymer films manufactured by NIPS were exposed to a $CHCl_3$ vapor for 5 h in order to promote the mobility of BCP chains until reaching the formation of the DG structure. Here, a continuous flow system was used to control the $CHCl_3$ vapor pressure (32 sccm $CHCl_3$+8 sccm N_2) in the SVA chamber as described previously [28]. Note that the temperature of the $CHCl_3$ tank was kept at 20°C during the SVA process.

4.4. AFM and SEM Imaging. Atomic force microscopy (AFM Nano-Observer, CSInstruments) was used in tapping mode to characterize the surface morphology of PS-*b*-P2VP-*b*-PEO/PS-*b*-PEO films. Silicon cantilevers (PPP-NCH, Nanosensors) with a typical tip radius of ~5 nm were used. The resonance frequency of cantilevers was ~235 kHz. Scanning electron microscopy (SEM, Hitachi S-4800) was used at an accelerating voltage of 5 kV to acquire top view and cross-section images of both asymmetric thick films and monoliths.

4.5. GISAXS Characterizations. GISAXS experiments were performed on the Dutch-Belgian Beamline (DUBBLE) at the European Synchrotron Radiation Facility (ESRF) station BM26B in Grenoble [29]. A monochromatic beam of 12 keV was set using a Si (111) double crystal monochromator. The sample (typical size of 150 mm^2) was shone with the X-ray beam with an incidence angle of 0.2° that was above the critical angle of the polymer, ensuring full penetration of the X-ray beam in the material and hence analyzing the full volume of the sample [30]. The 2D scattering patterns were collected with a PILATUS3 S 1 M detector. The scattering vector and the sample-to-detector distance were calibrated using silver behenate as standard, obtaining a sample-to-detector distance of 7500 mm.

4.6. Water Flux Performances. To perform the water flux tests, the blended PS-*b*-P2VP-*b*-PEO/PS-*b*-PEO films generated by NIPS-SVA (0 h and 5 h) were deposited on a sacrificial (water-soluble) 100 nm-thick PEDOT:PSS layer in order to facilitate the removal of the terpolymer layer from the substrate. For that purpose, silicon pieces were treated by an oxygen plasma in a home-made chamber (plasma conditions: 45 W, 75 mTorr O_2, 10 min) prior to the deposition of the sacrificial PEDOT:PSS layer (spin-coat conditions: speed = 1000 rpm, acceleration = 500 $rpm.s^{-1}$, and time = 90 s). The

water permeability of the different PS-*b*-P2VP-*b*-PEO/PS-*b*-PEO films was measured in a 10 mL filtration cell (Amicon 8010 stirred cell) connected to a water reservoir and a compressed air line. The measurements were performed on 2.5 cm-diameter PS-*b*-P2VP-*b*-PEO/PS-*b*-PEO material discs supported by a high-permeable hydrophilic PVDF material [24] at pressures between 0.5 and 2 bar. The mass of water passing through the stacked materials (permeate) was recorded using a connected balance at regular time intervals for 10 min. The water temperature was maintained at 20°C during the measurements, while the error bars were calculated from 3 different samples. In order to avoid a nonlinear behavior of the water flux with the increase in pressure drop, a transmembrane pressure of 2.5 bar was systematically applied during 10 min on each terpolymer film prior to measurements to determine their permeability performance.

Data Availability

All the data used in this work have been provided in the text and in the supplementary materials. Any request could be directed to the corresponding author (email: karim.aissou@umontpellier.fr).

Conflicts of Interest

The authors declare that they have no conflicts of interest.

Acknowledgments

This work was performed within the support of the ANR JCJC AFM_Ring Project (grant ANR-18-CE09-00xx) of the French Agence Nationale de la Recherche. Open Access funding was enabled and organized by the COUPERIN CY23.

Supplementary Materials

Distribution of P2VP/PEO nanodomains generated by NIPS. Large view AFM topographic image and 2D-GISAXS pattern performed on PS-*b*-P2VP-*b*-PEO/PS-*b*-PEO monoliths generated by NIPS-SVA (5 h). AFM topographic and SEM images as well as 2D-GISAXS pattern performed on asymmetric PS-*b*-P2VP-*b*-PEO/PS-*b*-PEO tick films generated by NIPS-SVA (45 min). *(Supplementary Materials)*

References

[1] A. El Sachat, J. Spièce, C. Evangeli et al., "Nanoscale mapping of thermal and mechanical properties of bare and metal-covered self-assembled block copolymer thin films," *ACS Applied Polymer Materials*, vol. 2, no. 2, pp. 487–496, 2020.

[2] T. Kobayashi, Y.-X. Li, A. Ono, X.-B. Zeng, and T. Ichikawa, "Gyroid structured aqua-sheets with sub-nanometer thickness enabling 3D fast proton relay conduction," *Chemical Science*, vol. 10, no. 25, pp. 6245–6253, 2019.

[3] M. A. Morris, H. An, J. L. Lutkenhaus, and T. H. Epps, "Harnessing the power of plastics: nanostructured polymer systems in lithium-ion batteries," *ACS Energy Letters*, vol. 2, no. 8, pp. 1919–1936, 2017.

[4] Y. Shi, L. Peng, Y. Ding, Y. Zhao, and G. Yu, "Nanostructured conductive polymers for advanced energy storage," *Chemical Society Reviews*, vol. 44, no. 19, pp. 6684–6696, 2015.

[5] L. Yan, C. Rank, S. Mecking, and K. I. Winey, "Gyroid and other ordered morphologies in single-ion conducting polymers and their impact on ion conductivity," *Journal of the American Chemical Society*, vol. 142, no. 2, pp. 857–866, 2020.

[6] V. Abetz, "Isoporous block copolymer membranes," *Macromolecular Rapid Communications*, vol. 36, no. 1, pp. 10–22, 2015.

[7] S. P. Nunes, "Block copolymer membranes for aqueous solution applications," *Macromolecules*, vol. 49, no. 8, pp. 2905–2916, 2016.

[8] Y. Zhang, J. L. Sargent, B. W. Boudouris, and W. A. Phillip, "Nanoporous membranes generated from self-assembled block polymer precursors: Quo Vadis?," *Journal of Applied Polymer Science*, vol. 132, no. 21, 2015.

[9] N. Hampu, J. R. Werber, W. Y. Chan, E. C. Feinberg, and M. A. Hillmyer, "Next-generation ultrafiltration membranes enabled by block polymers," *ACS Nano*, vol. 14, no. 12, pp. 16446–16471, 2020.

[10] J. Feng, J. Fu, X. Yao, and Y. He, "Triply periodic minimal surface (TPMS) porous structures: from multi-scale design, precise additive manufacturing to multidisciplinary applications," *International Journal of Extreme Manufacturing*, vol. 4, no. 2, article 022001, 2022.

[11] J.-W. Luo, L. Chen, T. Min, F. Shan, Q. Kang, and W. Tao, "Macroscopic transport properties of gyroid structures based on pore-scale studies: permeability, diffusivity and thermal conductivity," *International Journal of Heat and Mass Transfer*, vol. 146, article 118837, 2020.

[12] E. J. W. Crossland, M. Kamperman, M. Nedelcu et al., "A bicontinuous double gyroid hybrid solar cell," *Nano Letters*, vol. 9, no. 8, pp. 2807–2812, 2009.

[13] S. Choudhury, M. Agrawal, P. Formanek et al., "Nanoporous cathodes for high-energy Li-S batteries from gyroid block copolymer templates," *ACS Nano*, vol. 9, no. 6, pp. 6147–6157, 2015.

[14] J. G. Werner, G. G. Rodriguez-Calero, H. D. Abruna, and U. Wiesner, "Block copolymer derived 3-D interpenetrating multifunctional gyroidal nanohybrids for electrical energy storage," *Energy & Environmental Science*, vol. 11, no. 5, pp. 1261–1270, 2018.

[15] S. Park, Y. Kim, H. Ahn, J. H. Kim, P. J. Yoo, and D. Y. Ryu, "Giant gyroid and templates from high-molecular-weight block copolymer self-assembly," *Scientific Reports*, vol. 6, no. 1, article 36326, 2016.

[16] A. J. Meuler, M. A. Hillmyer, and F. S. Bates, "Ordered network mesostructures in block polymer materials," *Macromolecules*, vol. 42, no. 19, pp. 7221–7250, 2009.

[17] K. Aissou, M. Mumtaz, N. Demazy, G. Pécastaings, G. Fleury, and G. Hadziioannou, "Periodic bicontinuous structures formed on the top surface of asymmetric triblock terpolymer thick films," *ACS Macro Letters*, vol. 8, no. 8, pp. 923–930, 2019.

[18] L. Li, P. Szewczykowski, L. D. Clausen, K. M. Hansen, G. E. Jonsson, and S. Ndoni, "Ultrafiltration by gyroid nanoporous polymer membranes," *Journal of Membrane Science*, vol. 384, no. 1-2, pp. 126–135, 2011.

[19] L. Li, L. Schulte, L. D. Clausen, K. M. Hansen, G. E. Jonsson, and S. Ndoni, "Gyroid nanoporous membranes with tunable permeability," *ACS Nano*, vol. 5, no. 10, pp. 7754–7766, 2011.

[20] D. S. Marques, U. Vainio, N. M. Chaparro et al., "Self-assembly in casting solutions of block copolymer membranes," *Soft Matter*, vol. 9, no. 23, p. 5557, 2013.

[21] B. Lee, I. Park, J. Yoon et al., "Structural analysis of block copolymer thin films with grazing incidence small-angle X-ray scattering," *Macromolecules*, vol. 38, no. 10, pp. 4311–4323, 2005.

[22] I. Park, B. Lee, J. Ryu et al., "Epitaxial phase transition of polystyrene-b-Polyisoprene from hexagonally perforated layer to gyroid phase in thin film," *Macromolecules*, vol. 38, no. 25, pp. 10532–10536, 2005.

[23] K. Aissou, M. Mumtaz, H. Bouzit et al., "Bicontinuous network nanostructure with tunable thickness formed on asymmetric triblock terpolymer thick films," *Macromolecules*, vol. 52, no. 12, pp. 4413–4420, 2019.

[24] K. Aissou, H. Bouzit, F. Krusch et al., "Asymmetric solvent-annealed triblock terpolymer thick films topped by a hexagonal perforated lamellar nanostructure," *Macromolecular Rapid Communications*, vol. 43, no. 2, article 2100585, 2022.

[25] K. Aissou, M. Mumtaz, G. Portale et al., "Templated sub-100-nm-thick double-gyroid structure from Si-containing block copolymer thin films," *Small*, vol. 13, no. 20, article 1603777, 2017.

[26] M. W. Matsen, "Cylinder ↔ gyroid epitaxial transitions in complex polymeric liquids," *Physical Review Letters*, vol. 80, p. 4470, 1998.

[27] R. M. Dorin, W. A. Phillip, H. Sai, J. Werner, M. Elimelech, and U. Wiesner, "Designing block copolymer architectures for targeted membrane performance," *Polymer*, vol. 55, no. 1, pp. 347–353, 2014.

[28] K. W. Gotrik, A. F. Hannon, J. G. Son, B. Keller, A. Alexander-Katz, and C. A. Ross, "Morphology control in block copolymer films using mixed solvent vapors," *ACS Nano*, vol. 6, no. 9, pp. 8052–8059, 2012.

[29] G. Portale, D. Hermida-Merino, and W. Bras, "Polymer research and synchrotron radiation perspectives," *European Polymer Journal*, vol. 81, pp. 415–432, 2016.

[30] I. Saito, T. Miyazaki, and K. Yamamoto, "Depth-resolved structure analysis of cylindrical microdomain in block copolymer thin film by grazing-incidence small-angle X-ray scattering utilizing low-energy X-rays," *Macromolecules*, vol. 48, no. 22, pp. 8190–8196, 2015.